# Polyphenol-Inspired Facile Construction of Smart Assemblies for ATP- and pH-Responsive Tumor MR/Optical Imaging and Photothermal Therapy

*Xiao-Rong Song, Shi-Hua Li, Jiayong Dai, Liang Song, Guoming Huang, Ruhui Lin, Juan Li,* Gang Liu, and Huang-Hao Yang**

*Smart assemblies have attracted increased interest in various areas, especially in developing novel stimuli-responsive theranostics. Herein, commercially available, natural tannic acid (TA) and iron oxide nanoparticles ($Fe_3O_4$ NPs) are utilized as models to construct smart magnetic assemblies based on polyphenol-inspired NPs–phenolic self-assembly between NPs and TA. Interestingly, the magnetic assemblies can be specially disassembled by adenosine triphosphate, which shows a stronger affinity to $Fe_3O_4$ NPs than that of TA and partly replaces the surface coordinated TA. The disassembly can further be facilitated by the acidic environment hence causing the remarkable change of the transverse relaxivity and potent "turn-on" of fluorescence (FL) signals. Therefore, the assemblies for specific and sensitive tumor magnetic resonance and FL dual-modal imaging and photothermal therapy after intravenous injection of the assemblies are successfully employed. This work not only provides understandings on the self-assembly between NPs and polyphenols, but also will open new insights for facilely constructing versatile assemblies and extending their biomedical applications.*

X.-R. Song, S.-H. Li, J. Dai, L. Song, Dr. G. Huang, Prof. J. Li, Prof. H.-H. Yang
The Key Lab of Analysis and Detection Technology for Food Safety of the MOE
State Key Laboratory of Photocatalysis on Energy and Environment
College of Chemistry
Fuzhou University
Fuzhou 350108, China
E-mail: lijuan@fzu.edu.cn; hhyang@fzu.edu.cn

Prof. G. Liu
State Key Laboratory of Molecular Vaccinology and Molecular Diagnostic
Center for Molecular Imaging and Translational Medicine
School of Public Health
Xiamen University
Xiamen 361005, China

R. Lin
Academy of
Intergrative Medicine
Biomedical Research Center
Fujian University of Tranditional Chinese Medicine
Fuzhou 350122, China

DOI: 10.1002/smll.201603997

## 1. Introduction

Remarkable advanced progress in nanomedicine has shown great prospects in fighting cancers through integrating multiple imaging and therapeutic technologies in tandem.[1] Ideally, the nanomaterials intended for medicine should be biocompatible and manifest high tumor accumulation as well as specific imaging and drug release in the desired site without causing serious side effects. However, it is still an impressive challenge to specially differentiate tumors from normal tissues or achieve target imaging and therapy.[2] In line with this effort, recent surge in nanomedicine, to a certain extent, has shed light on activatable systems which can endow highly specific imaging and on-demand therapy.[3] These systems are relied on the fact that tumor featured with uncontrolled growth always exhibits rapid angiogenesis with some characteristics, such as altered expression profiles of certain local enzymes, aberrant hypoxia, and acidic pH condition.[4] Due to these commonalities existed in tumor microenvironment, responsive theranostics that can differentiate healthy and diseased tissue would be realizable and beneficial for tumor specific imaging and therapy.

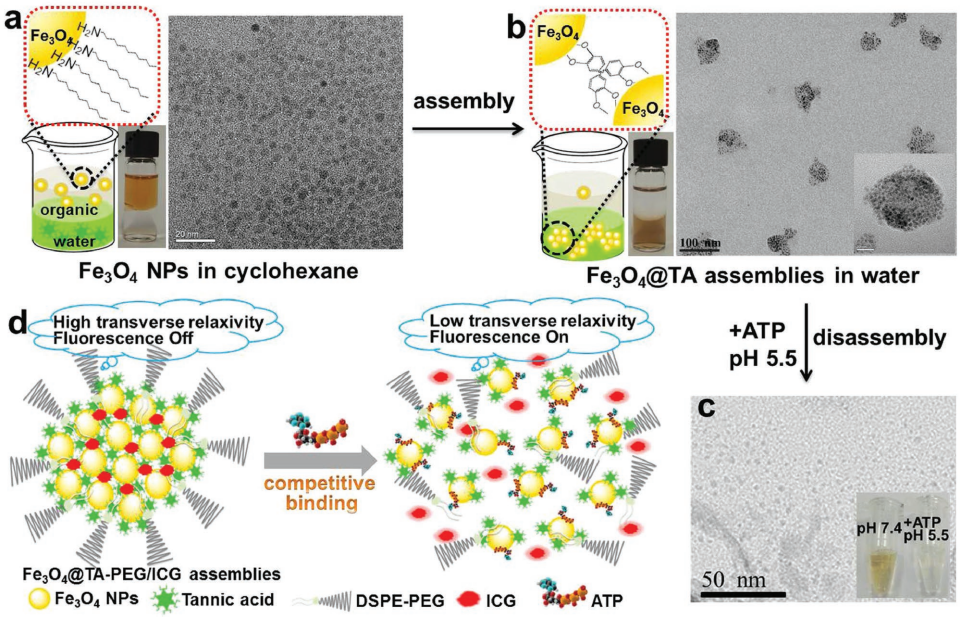


**Figure 1.** Construction of the smart assemblies and schematic illustration of the ATP-responsive disassembly. a) Hydrophobic $Fe_3O_4$ NPs and the TEM image. b) Water-dispersive $Fe_3O_4$@TA assemblies and the TEM image. c) The TEM image of the assemblies after treating with ATP. Inset: photographs of aqueous solution of the assemblies at different conditions. d) Schematic illustration of the disassembly process.

In order to maximize the potency of such stimuli-responsive systems, it is of great importance to effectively stimulate them and further generate detectable signals and achieve therapeutic purposes as well. Among the stimulus, acidic pH in tumor microenvironment has been widely exploited for responsive theranostic with broad applicability.[3b,5] Besides, great attentions also have been paid to intracellular biomolecules, such as adenosine triphosphate (ATP), which is the "molecular unit of currency" for intracellular energy transfer and exists in intracellular cytosol at a much higher concentration ($1 \times 10^{-3}$ to $10 \times 10^{-3}$ M) than that in the body fluids ($<0.5 \times 10^{-3}$ M).[6] Furthermore, upregulated ATP level was found in cancerous tissues.[7] After determining certain stimulus, decent ligands with cleavable or conformation changeable moieties, degradable nanomaterials or functional assemblies always need to be delicately designed and synthesized to be susceptible to the specific stimulation.[8] However, the complex design and tedious synthesis would restrict their applications and even sometimes induce a toxic effect. In this regard, smart theranostics made directly from commercially available molecules/nanomaterials or even clinical agents would be imperative to avoid complex synthetic procedures as well as to improve biocompatibility and facilitate their potential clinical translation.[1d,9]

Plant polyphenols are biocompatible molecules that possess antioxidant activity and can coordinate with various metal ions due to the multiple catechols and pyrogallol groups within molecules.[10] Polyphenol-inspired chemistry, based on the robust coordination between metal ion and phenols, has opened new avenues for the surface functionalization of various objects and constructing metal–phenolic network capsules.[11] Besides, polyphenols not only can be used as reductants for the green synthesis of metal nanoparticles (NPs) but also act as structure directing ligands for synthesizing NPs with special morphologies.[12] However, the understandings on the assembly behavior of polyphenols and NPs are still rather limited. In this work, we utilized polyphenols as phase transfer agents to transfer hydrophobic magnetic NPs into aqueous solution, at the same time, the polyphenols can drive the self-assembly of NPs into assemblies. A more important design of the assemblies is their ATP-responsive and acidic pH-facilitated disassembly capability that specially generates magnetic resonance (MR) and fluorescence (FL) signals for tumor environment responsive MR/FL dual-modal imaging and photothermal therapy (PTT) (**Figure 1**). To the best of our knowledge, this is the first attempt to construct NPs–polyphenols based smart self-assemblies for stimuli-responsive theranostics.

## 2. Results and Discussion

To construct the smart magnetic assemblies, tannic acid (TA), a ubiquitous polyphenol in plants, and super-paramagnetic iron oxide NPs ($Fe_3O_4$ NPs) were used as models to firstly construct $Fe_3O_4$@TA assemblies through one step assembly during phase transfer. $Fe_3O_4$ NPs covered hydrophobic ligands were well-dispersed in cyclohexane and had uniform size of 4.3 ± 0.4 nm as revealed from transmission electron microscopy (TEM) results in Figure 1a and Figure S1 (Supporting Information). A clear phase transfer of NPs from the organic solvent to aqueous solution was observed after introducing the aqueous solution of TA, followed by sonication and gentle stirring for 12 h (Figure 1b). At the same time, interestingly, TA and $Fe_3O_4$ NPs can be self-assembled into well water-dispersive $Fe_3O_4$@TA assemblies in a high yield. TEM images indicated that $Fe_3O_4$@TA assemblies had diameters of 76.0 ± 11.1 nm (Figure 1b), which was confirmed

  

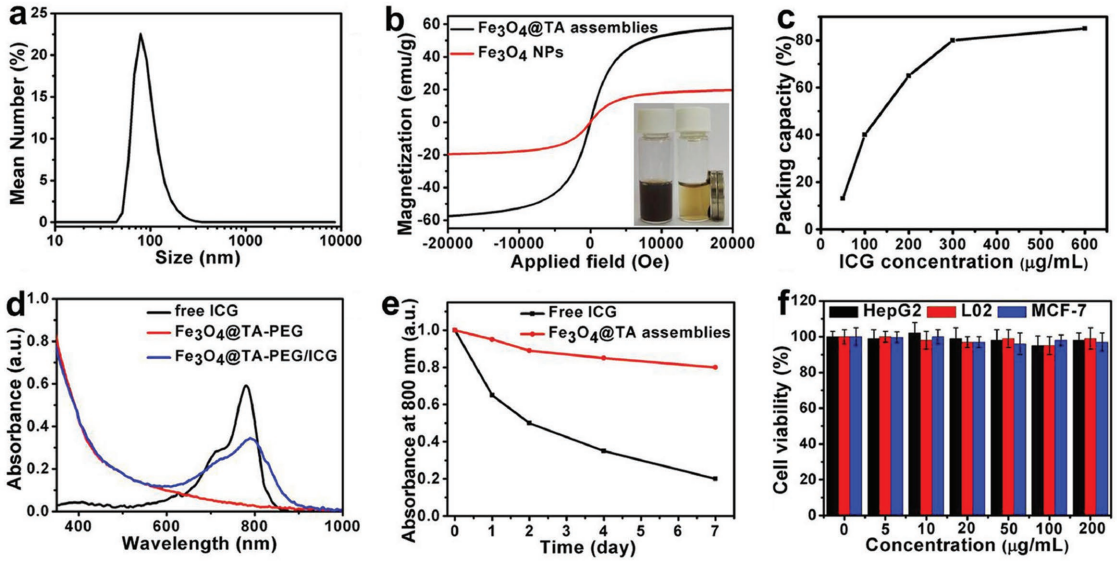


**Figure 2.** a) DLS data of the assemblies in aqueous solution. b) The field-dependent magnetization curve of $Fe_3O_4$@TA assemblies and individual $Fe_3O_4$ NPs. Inset: images of the assemblies without and with magnet. c) ICG packing efficiency with different concentrations of ICG. d) Absorbance spectra of free ICG, $Fe_3O_4$@TA-PEG, and $Fe_3O_4$@TA-PEG/ICG assemblies. e) Time evolution of absorbance at 800 nm of free ICG and $Fe_3O_4$@TA-PEG/ICG assemblies within 7 d. f) Relative cell viability of HepG2, L02, and MCF-7 after treating with different concentrations of the assemblies for 24 h.

by dynamic light scattering (DLS) data (**Figure 2**a; Figure S1, Supporting Information). The field-dependent magnetization curves showed that $Fe_3O_4$@TA assemblies had higher magnetic saturation value of about 58 emu $g^{-1}$ than that of individual $Fe_3O_4$ NPs (about 20 emu $g^{-1}$) due to the coupling effect of magnetic dipoles in the assemblies (Figure 2b),[13] presaging their potential applications in magnetic targeting and MR imaging as well as in magnetic separation.[14]

We next carried out control experiments to study the key factors that significantly affect the self-assembly process. When using 3,4-dihydroxyhydrocinnamic acid (DHCA) or salvianolic acid B (SAB) as surface exchange ligands, as shown in Figure S2 (Supporting Information), only unassembled NPs dispersed in aqueous solution were obtained, indicating neither molecules containing single catechol group (i.e., DHCA) nor that with multiple catechol and pyrogallol groups but smaller molecule size (i.e., SAB) can impel the assembly process.[15] We also used TA to transfer another hydrophobic $Fe_3O_4$ NPs with larger size (about 15 nm diameter) into aqueous phase, whereas microscale aggregates were observed from the TEM results (Figure S3, Supporting Information). By contrast, 5 nm CdSe quantum dots not only can be phase transferred by TA into aqueous phase with a high yield, but also can form CdSe@TA assemblies with similar size to $Fe_3O_4$@TA assemblies (Figure S4, Supporting Information). These results imply that polyphenols with multiple binding sites for NPs can drive the self-assembly of NPs. Besides, the forming of the nanoscale assemblies, to some extents, is contingent on the spatial match between the NPs size and interparticle spacing originated by polyphenols, which draws new insights into the design and synthesis of proper polyphenols and NPs for constructing NPs–polyphenols based assemblies.[10a,b,16]

To prove that $Fe_3O_4$@TA assemblies can be served as a multifunctional theranostic platform, polyethylene glycol-modified distearyl phosphatidyl ethanolamine (DSPE-PEG, $M_W$ 2000) and indocyanine green (ICG) were simultaneously packed on $Fe_3O_4$@TA assemblies to form $Fe_3O_4$@TA-PEG/ICG assemblies, which may be attributed to the rich $\pi$ systems and hydroxyl groups in TA that allow its noncovalent binding with DSPE-PEG and ICG through $\pi$–$\pi$ stacking and hydrogen-bond interaction. We also found that the packing efficiency of ICG on the assemblies was increased with increasing ICG concentration (Figure 2c). After packing with ICG, the assemblies showed a characteristic ICG absorbance at around 800 nm (Figure 2d). The assemblies loaded with 65% (w/w) of ICG were used throughout the paper without further notice. The hydrodynamic diameter of $Fe_3O_4$@TA-PEG/ICG assemblies was measured to be 78.8 ± 12.5 nm by DLS analysis. Notably, the photostability of ICG in the assemblies was apparently improved compared to free ICG (Figure 2e). We then studied cytotoxicity of the assemblies using L02, HepG2, and MCF-7 cells. As shown in Figure 2f, the assemblies showed insignificant effect on the viability of all three types of cells, suggesting their good cytocompatibility.

One pivotal design of the assemblies is their ATP-responsive disassembly capability, since ATP was reported to have strong binding affinity to $Fe_3O_4$ NPs.[17] To appraise the validity, the transverse relaxation rate ($1/T_2$) and MR images of assemblies were recorded before and after exposing to ATP. As shown in **Figure 3**a, aqueous solution of $Fe_3O_4$@TA-PEG/ICG assemblies exhibited a forceful MR contrast capacity with the transverse relaxivity ($r_2$) of 251.2 $mM^{-1}$ $s^{-1}$, which is much higher than that of monodisperse $Fe_3O_4$ NPs.[18] In the meanwhile, MR images were gradually darkened with the increase of the concentration of the assemblies (Figure 3b). Interestingly, $r_2$ value of the assemblies was significantly decreased to 31.85 $mM^{-1}$ $s^{-1}$ after being exposed to $10 \times 10^{-3}$ M ATP for 24 h. To explain the remarkable change of transverse

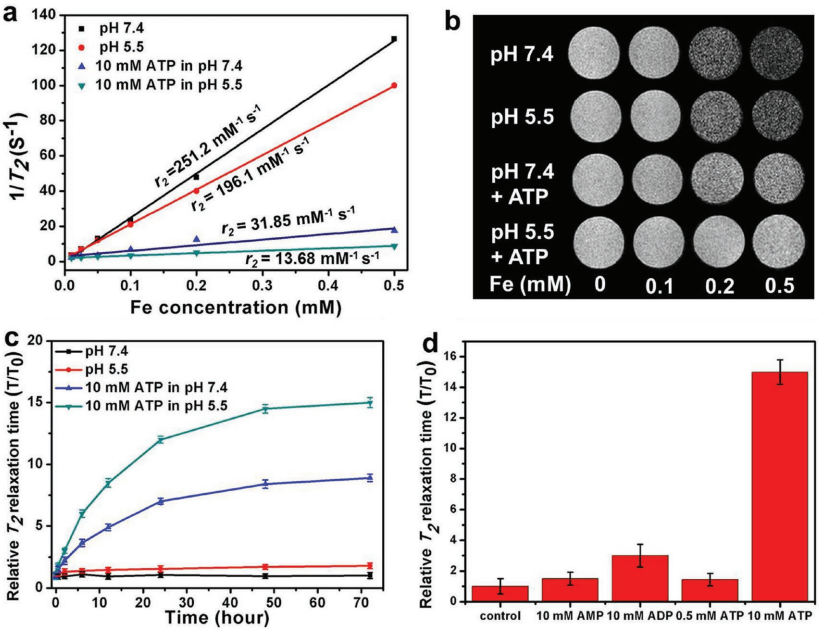


**Figure 3.** a) The transverse relaxivity ($r_2$), b) $T_2$-weighted MR images, and c) Time evolution of relative $T_2$ relaxation time of $Fe_3O_4$@TA-PEG/ICG assemblies at 0.5-T MR scanner under different conditions. d) Relative $T_2$ relaxation time of the assemblies after different treatments.

relaxivity, TEM image of the assemblies after treating with ATP showed only individual small $Fe_3O_4$ NPs, indicating the assemblies were disassembled by ATP (Figure 1c). Therefore, it is reasonable that the assemblies exhibited larger transverse relaxivity than that after disassembly, since the $r_2$ relaxivity of magnetic NPs would be significantly enhanced when they formed aggregates.[19]

The ATP-responsive disassembly process was further examined under acidic pH condition (pH = 5.5). As shown in Figure 3a, the transverse relaxivity was decreased to 13.68 mM$^{-1}$ s$^{-1}$ in a shorter period than that required for single ATP treatment, indicating the ATP-responsive disassembly process was distinctly facilitated and accelerated under cooperation of ATP and pH = 5.5 environment compared to single ATP treatment (Figure 3c). However, the assemblies displayed only an insignificant variation of transverse relaxivity in pH = 5.5 condition compared to that in pH = 7.4 condition. As shown in Figure S5 (Supporting Information), the assemblies also showed pH-facilitated disassembly ability in pH = 6.5 condition. The promotion of the disassembly process in weak acid condition would be caused by the protonation of hydroxyl groups in TA, leading to the weakening of metal—polyphenols coordination. So the loosened assemblies would exhibit decreased $T_2$ relaxivity and would be more easily to be disassembled by ATP. Besides, negligible changes of transverse relaxivity were observed when replacing $10 \times 10^{-3}$ M ATP with same concentration of adenosine diphosphate and adenosine monophosphate in the systems, as well as when using a lower concentration of ATP ($0.5 \times 10^{-3}$ M), indicating that the assemblies would be specially disassembled by intracellular ATP (Figure 3d). More importantly, we also found that $Fe_3O_4$@TA-PEG/ICG assemblies displayed very weak FL due to the partly FL quenching effect of $Fe_3O_4$ NPs to ICG because of their close distance (Figure S6, Supporting Information). Notably, strong FL was observed after exposing to $10 \times 10^{-3}$ M ATP, showing potent responsive "turn-on" of FL signals.

In addtion, the stability of the assemblies in different solution was also studied by DLS. As shown in Figure S7 (Supporting Information), the size of the assemblies remained unchanged in all condition, indicating their excellent stability without disassembly even in complex condition. We next carried out cell imaging experiment with the aim of examining their cell uptake and disassembly properties. As shown in **Figure 4**a, the cells treated with $Fe_3O_4$@TA-PEG/ICG assemblies for 3 h showed a significant darkening effect with 63.7% dropping of $T_2$-weighted signal intensity compared to that of cells without treatment. Interestingly, $T_2$-weighted signal intensity of the cells showed only 18.6% dropping from the baseline after prolonging the incubation time to 8 h, indicating that the assemblies were first

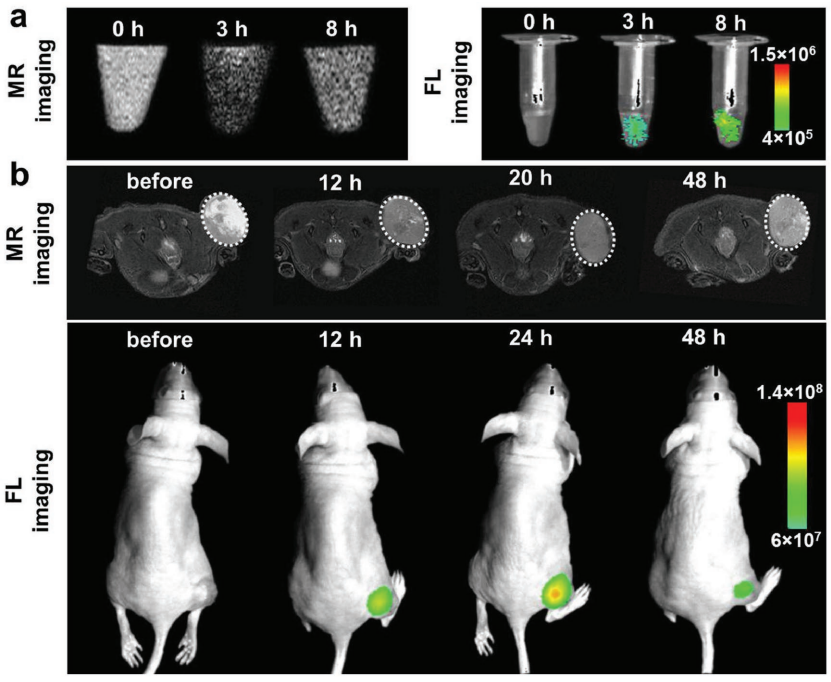


**Figure 4.** a) $T_2$-weighted MR images and FL images of cells after incubating with the assemblies for different time. b) $T_2$-weighted MR images and FL images of HepG2 tumor-bearing mice after intravenous injection of the assemblies.

uptake into cells followed by disassembly within cell environment. The FL imaging results also confirmed the similar phenomenon. The FL intensity of cells showed about six times enhancement and eight times enhancement after incubating with the assemblies for 3 and 8 h as compared to that without treatment, respectively, indicating the disassembly process was facilitated by prolonging the incubation time.

Hereto, the advent of the self-assembly and disassembly process became comprehensible. Due to their multiple catechol groups, TA can exchange the surface hydrophobic ligands of $Fe_3O_4$ NPs and further self-assemble with $Fe_3O_4$ NPs to form assemblies. Importantly, this assembly strategy would be universally applicable to prepare other small NPs assemblies, such as above described CdSe@TA assemblies. Since ATP showed stronger binding affinity than that of TA to $Fe_3O_4$ NPs, especially in acidic condition, where some of the hydroxyl groups in TA would be protonated and metal–polyphenols coordination was weakened, ATP would partly replace surface TA and cause the subsequent disassembly.[11c] This ATP-responsive and pH-facilitated disassembly property makes the assemblies vastly suitable for specific imaging in tumor environment, where provides enough ATP and acidic condition.[20] It is valuable to mention that this disassembly capacity may also provide a strategy for designing renal clearable theranostics without long-term toxicity due to the ultrasmall size of disassembled NPs.[21]

We next utilized the assemblies for in vivo MR/FL dual-modal tumor imaging. $T_2$-weight MR images and FL images of mice were performed after intravenous injection with the $Fe_3O_4$@TA-PEG/ICG assemblies for different temporal points. As shown in Figure 4a and Figure S8 (Supporting Information), a gradual contrast enhancement in tumor areas was observed and a clearly darkened MR image in tumor can be seen at 20 h with 46.6% dropping of signal intensity compared to that before treatment, indicating the gradual accumulation of the assemblies in tumor. Particularly, the contrast capability was decreased post injection for 48 h, only 16.9% dropping of signal intensity compared to that before injection, suggesting the assemblies were disassembled into individual small NPs with poor contrast capability and some small $Fe_3O_4$ NPs could possibly be cleared out from the body. Moreover, FL images of tumor also showed seven times enhancement of signals post injection for 20 h as compared to that without injection. At 48 h postinjection, the intensity of FL in tumor was decreased but still can be observed. In order to look insights into the disassembly process in tumor, we also carried out the FL imaging of mice after intratumor injection of the assemblies. As shown in Figure S9 (Supporting Information), FL images of tumor exhibited no signal just after injection, whereas FL signals showed gradual increase and reached maximum after injection for 12 h, followed by the slow decrease. The gradual restoration of FL indicated the in vivo disassembly was triggered slowly, ensuring the accumulation and disassembly of the assemblies in tumor can be tracked in MR images. Therefore, $Fe_3O_4$@TA-PEG/ICG assemblies can be successfully accumulated in tumor area, and exhibited tumor environment responsive disassembly capability, allowing for specific tumor MR/FL dual-modal imaging.

The pharmacokinetic studies of $Fe_3O_4$@TA-PEG/ICG assemblies were next carried out. The half-life of $Fe_3O_4$@TA-PEG/ICG assemblies in blood was determined to be ≈2.53 h (Figure S10, Supporting Information). In order to further study the biodistribution of the assemblies in vivo, major organs from mice treated without and with the assemblies for different times were collected for inductively coupled plasma atomic emission spectrometry (ICP-AES) measurement of iron concentrations. As shown in Figure S11 (Supporting Information), iron contents in liver, spleen, and tumor were obviously elevated compared to that in other organs after intravenous injection for 1 d. Interestingly, the iron contents in organs at 7 d decreased significantly compared to that at 1 d, indicating the gradual clearance of iron from mice. More in-depth studies will be done to investigate the clearance mechanism.

PTT is a noninvasive therapeutic method with the assistance of PTT agents and near-infrared (NIR) laser irradiation.[22] By virtue of strong NIR absorbance of the assemblies, their photothermal performance was studied. From **Figure 5**a,b, the temperatures of aqueous solution containing $Fe_3O_4$@TA-PEG/ICG assemblies were obviously elevated upon 808 nm laser irradiation (1 W $cm^{-2}$, 10 min). By contrast, $Fe_3O_4$@TA plus NIR laser and single NIR laser both can't induce the dramatic increase of water temperature, suggesting that the photothermal effect was assigned to ICG. Notably, the solution temperature reached 53 °C after treating with the assemblies containing 10 μg $mL^{-1}$ ICG plus laser exposure for 10 min. As shown in Figure S12 (Supporting Information), the photothermal conversion efficiency of $Fe_3O_4$@TA-PEG/ICG assemblies was calculated to be 19.1%. The excellent photothermal effect of the assemblies prompted us to investigate their PTT ability in vitro. As expect, increasing the concentration of $Fe_3O_4$@TA-PEG/ICG assemblies or NIR laser irradiation time induced the gradual decrease of cell viability as revealed from propidium iodide (PI) staining experiments (Figure 5c; Figure S13, Supporting Information). Significantly, 80% cell death was detected by treating with the assemblies containing 10 μg $mL^{-1}$ ICG plus 10 min laser irradiation (Figure 5d). However, only assemblies or NIR laser treated cells showed negligible cell death. These results indicated an excellent PTT effect of $Fe_3O_4$@TA-PEG/ICG assemblies in vitro.

The tumor environment responsiveness and excellent PTT effect in vitro of the assemblies encouraged us to further investigate their application for in vivo imaging guided cancer therapy. The thermal imaging was firstly carried out to examine their photothermal performance in vivo after intravenous injection with $Fe_3O_4$@TA-PEG/ICG assemblies for 24 h under laser irradiation (808 nm). It was shown that the temperature in tumor region exhibited 20 °C increase within 5 min, while tumor in mice treated without the assemblies showed no obvious temperature increase (Figure 5e,f). Tumor bearing mice were then divided into four groups, i.e., control group, $Fe_3O_4$@TA-PEG assemblies group, $Fe_3O_4$@TA-PEG/ICG group, and $Fe_3O_4$@TA-PEG/ICG assemblies plus NIR laser group when the tumor size reached about 80 $mm^3$. It should be noted that mice treating with the assemblies plus NIR irradiation remained neither obvious weight drop nor

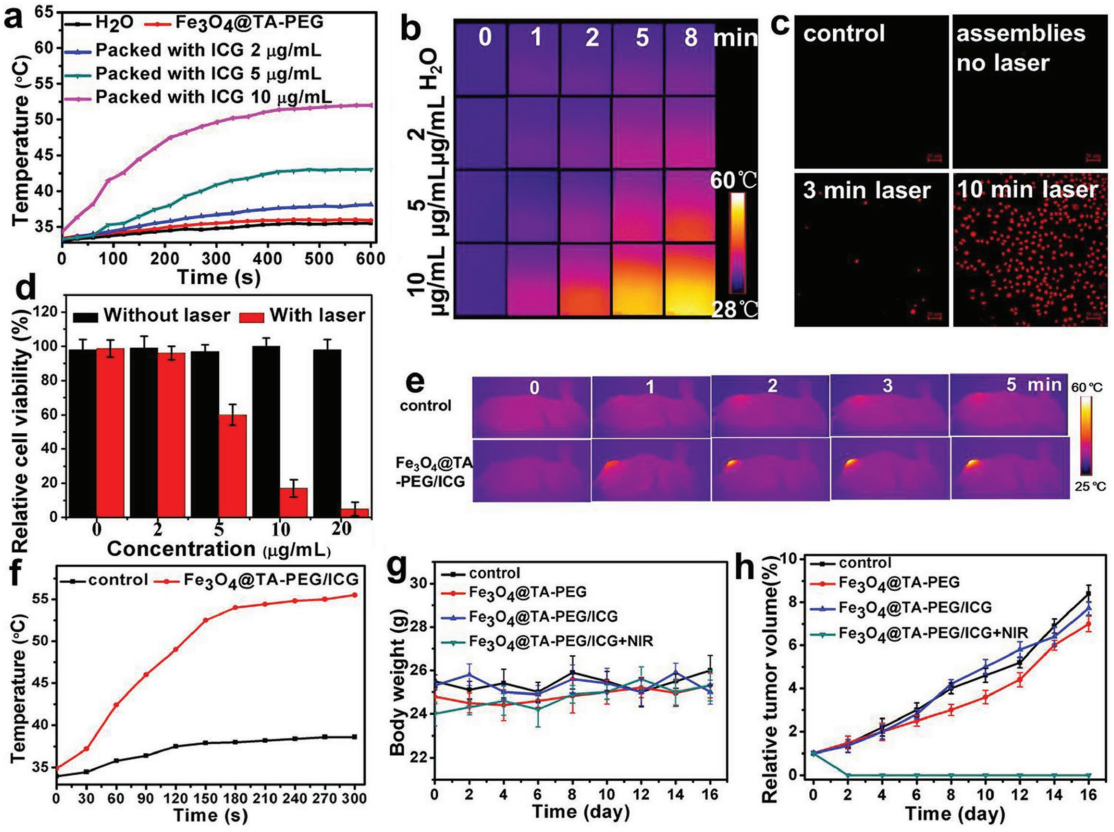


**Figure 5.** a) Photothermal heating curves and b) corresponding IR thermal images of the assemblies with different ICG concentrations under laser irradiation (808 nm, 1 W $cm^{-2}$). c) CLSM PIs FL images of differently treated HepG2 cells. d) Cell viability of HepG2 cells exposed to different concentrations of the assemblies with or without laser irradiation. e) Time evolution of IR thermal images and f) corresponding temperature value of tumor-bearing mice exposed to NIR laser after intravenous injection with phosphate buffered saline (PBS) or the assemblies for 24 h. g) Time evolution of body weights of mice in different groups. h) Tumor growth curves of different groups after treatment.

overt damage in major organs, indicating the good biocompatibility of the assemblies (Figure 5g; Figure S14, Supporting Information). The tumor sizes were measured every other day with a caliper. Experimental results showed that tumors in mice treated with $Fe_3O_4$@TA-PEG/ICG assemblies plus NIR laser exhibited remarkable ablation with no tumor recurrence post treatment for 16 d (Figure 5h; Figure S15, Supporting Information). By contrast, tumors in other three groups showed rapid growth. In particular, results of hematoxylin and eosin (H&E) staining revealed that tumor cells in mice treated with the assemblies plus NIR irradiation showed distinct necrosis with irregularly shaped cells, while cells in control group displayed regularly shaped cell morphology (Figure S14, Supporting Information). Besides, H&E stained images of major organs collected from the mice after treating with the assemblies for 30 d still showed no obvious damage or pathological change (Figure S16, Supporting Information). These results suggested that $Fe_3O_4$@TA-PEG/ICG assemblies are biocompatible, and can be used as powerful PTT agents for tumor PTT.

## 3. Conclusion

In summary, we facilely developed biocompatible smart self-assemblies with tumor environment-responsive disassembly for theranostic applications based on the polyphenol-inspired self-assembly between NPs and polyphenols. It is worthy noted that the $Fe_3O_4$@TA-PEG/ICG assemblies exhibited ATP-responsive and pH-facilitated disassembly capabilities due to the competitive binding of ATP and TA to the surface of $Fe_3O_4$ NPs. Endowed with remarkable change of the transverse relaxivity and potent "turn-on" of FL signals during the disassembly process, the assemblies were successfully employed for effective tumor MR/FL dual-modal imaging guided PTT. In addition, these disassembly capacities may implement a strategy for designing renal clearable theranostics without long-term toxicity. By virtue of the polyphenol-inspired self-assembly, this study provides new insights for the versatile assembly of NPs and even the coassembly of different NPs with synergistic effect for multi-modal imaging and combination therapy.

## 4. Experimental Section

*Chemicals*: TA, DHCA, and SAB were purchased from Sinopharm Chemical Reagent Co. Ltd (China). The DSPE-PEG ($M_w$ 2000) was purchased from Xi'an Ruixi Biological Technology Co. Ltd (China). ICG was purchased from Sigma-Aldrich. All the other chemicals were of analytical grade and were used as received. Ultrapure water obtained from a Millipore water purification system (18.2 MΩ resistivity) was used in all runs.

*Apparatus*: Ultraviolet–visible–near-infrared light (UV–vis–NIR) absorption spectra were tested by using an SH-1000 Lab microplate reader (Corona Electric, Hitachinaka, Japan) at room temperature. A semiconductor laser unit (KS3-11312-110, BWT, Beijing Kaipulin Co. Ltd, China) was employed for photothermal irradiation. The thermal images were obtained using FLIR A35 thermal camera. The in vitro MR images and the transverse relaxation time were recorded at 0.5-T MR scanner (Shanghai Niumai Corporation Ration NM120-Analyst). The in vivo MR images were obtained using 7.0-T MR scanner (Bruker, Biospec 70/30 USR). The FL images of cells were taken on a confocal fluorescence microscope (CLSM) (Nikon C2). The in vivo FL images were taken on an SI Imaging Amix small animal imaging system (Spectral Instruments Imaging Co., USA).

*Preparation of $Fe_3O_4$@TA-PEG/ICG Assemblies*: $Fe_3O_4$ NPs dispersed in cyclohexane (500 μg $mL^{-1}$) were mixed with equal volume of aqueous solution of TA, followed by sonication and gentle stirring for 12 h. The resulting aqueous solution was collected and centrifuged for 10 min (at 10 000 rotations per minute (rpm)) to obtain $Fe_3O_4$@TA assemblies. $Fe_3O_4$@TA-PEG/ICG assemblies were further obtained by mixing $Fe_3O_4$@TA assemblies with DSPE-PEG and ICG for 12 h under dark condition, followed by centrifugation and washing.

*Measurement of Transverse Relaxation Time*: In a typical experiment of the test of transverse relaxation rate ($1/T_2$), aqueous solution of $Fe_3O_4$@TA-PEG/ICG assemblies with different iron concentrations were prepared and measured using a 0.5-T MR scanner. The relaxation rate $r_2$ was determined from the slope of $1/T_2$ values as the function of iron concentrations.

*Cellular Experiments*: For cytotoxicity assay, HepG2, MCF-7, and L02 cells were cultured in RPMI-1640 medium (Gibco) plus 10% fetal bovine serum (Gibco) at 37 °C in a humidified atmosphere with 5% $CO_2$. In a typical experiment of the cytotoxicity assay, MCF-7 cells were seeded in 96-well plates and incubated overnight at 37 °C in a humidified 5% $CO_2$ atmosphere. The cells were then incubated with 100 μL of various concentrations of $Fe_3O_4$@TA-PEG/ICG assemblies for 24 h at 37 °C in the dark. Cell viabilities were determined by CCK-8 according to the manufacture's protocol. For PI staining experiments, HepG2 cells were incubated with various concentrations of $Fe_3O_4$@TA-PEG/ICG assemblies for 4 h, followed by exposing to NIR laser irradiation (808 nm, 1 W $cm^{-2}$). Then the cells were imaged by CLSM after PI staining.

*In Vitro MR and FL Imaging*: HepG2 cells ($2 \times 10^5$) were incubated with $Fe_3O_4$@TA-PEG/ICG assemblies for different time. Then, the cells were washed three times with PBS and harvested by trypsinization. After the cells were transferred into a 1.5 mL microtube and centrifuged, the resulting sediments were re-suspended in 0.2 mL PBS for further MR and FL imaging.

*In Vivo MR and FL Imaging*: BALB/c nude mice (weight ≈25 g) were obtained from Shanghai SLAC laboratory Animal Co., Ltd. Tumor-bearing mice were prepared by subcutaneously injecting a suspension of $10^6$ HepG2 cells in PBS (100 μL) into the back of the hind leg. In a typical experiment, tumor-bearing mice were intravenously injected with $Fe_3O_4$@TA-PEG/ICG assemblies for different time, and then anesthetized with 1%–2% isoflurane mixed with pure oxygen via a nose cone before imaging. For in vivo MR imaging, the following parameters at 7.0-T MR scanner were adopted for $T_2$-weighted multislice spinecho images: TR/TE = 2500/35 ms, matrix = 256 × 256, 15 contiguous slices. For in vivo FL imaging, the following wavelengths were set: excitation: 740 nm, emission: 800 nm.

*In Vivo Biodistribution Study*: For the pharmacokinetic studies, blood of mice was collected at 0, 0.5, 1, 2, 6, 12, and 24 h after intravenous injection with the assemblies. Plasma was collected from blood sample by centrifugation at 1000 rpm for 5 min, followed by mixing with 70% nitric acid at room temperature for 24 h, and the supernatant was used for ICP-AES after diluting with 2% nitric acid. Fe contents in tissues including major organs and tumors were determined after injection with the assemblies for 1 and 7 d. Dissected tissues were weighed and homogenized. Mixture solution of nitric acid and hydrogen peroxide solution (6:1, v/v) was added to each tissue, followed by heating for 24 h at 120 °C. The resulting solutions were further centrifuged and the supernatant was diluted with 2% nitric acid to 10 mL for ICP-AES test. The Fe contents in tissues were calculated as milligram of Fe content per gram of tissue (Fe mg/Tissue g).

*In Vivo PTT*: All mice were divided into four groups with five mice per group when the tumor size reached about 80 $mm^3$. HepG2-tumor-bearing mice were intravenously injected with 100 μL of PBS, $Fe_3O_4$@TA-PEG assemblies, and $Fe_3O_4$@TA-PEG/ICG assemblies, respectively ($Fe_3O_4$@TA-PEG/ICG assemblies 10 mg $kg^{-1}$). After injections for 24 h, tumors were irradiated with NIR laser (808 nm, 1 W $cm^{-2}$) for 10 min. Infrared thermal Imaging system was performed for studying the in vivo photothermal effect. The tumor sizes were measured by a digital caliper every other day. The tumor volumes were calculated through the equation: volume = $ab^2/2$, where $a$ and $b$ are the maximum diameter and the minimum diameter of tumor respectively. Relative tumor volumes were calculated as $V/V_0$, where $V_0$ is the tumor volume when the treatment was initiated. The body weights of mice were also measured every other day.

*Histology Analysis*: Animals with tumors were sacrificed and major organs were collected after treatment for histological examination using H&E staining method.

All experiments involving animals were approved by the Animal Ethics Committee of Fujian Medical University.

## Supporting Information

*Supporting Information is available from the Wiley Online Library or from the author.*

## Acknowledgements

*This research was supported by the National Natural Science Foundation of China (Nos. U1505221, 21505021, 21622502, and 21475026), the Natural Science Foundation of Fujian Province of China (Nos. 2015H6011 and 2016J05035), the Program for Changjiang Scholars and Innovative Research Team in University (No. IRT15R11), and the Independent Research Project of State Key Laboratory of Photocatalysis on Energy and Environment (No. 2014B02).*

[1] a) F. Caruso, T. Hyeon, V. M. Rotello, *Chem. Soc. Rev.* **2012**, *41*, 2537; b) E. K. Chow, D. Ho, *Sci. Transl. Med.* **2013**, *5*, 216rv4; c) D. Yoo, J. H. Lee, T. H. Shin, J. Cheon, *Acc. Chem. Res.* **2011**, *44*,

  

863; d) S. Kunjachan, J. Ehling, G. Storm, F. Kiessling, T. Lammers, *Chem. Rev.* **2015**, *115*, 10907.
[2] a) D. Ling, M. J. Hackett, T. Hyeon, *Nat. Mater.* **2014**, *13*, 122; b) Y. Ma, J. Huang, S. Song, H. Chen, Z. Zhang, *Small* **2016**, *12*, 4936.
[3] a) A. P. Blum, J. K. Kammeyer, A. M. Rush, C. E. Callmann, M. E. Hahn, N. C. Gianneschi, *J. Am. Chem. Soc.* **2015**, *137*, 2140; b) S. Mura, J. Nicolas, P. Couvreur, *Nat. Mater.* **2013**, *12*, 991; c) S. Wang, P. Huang, X. Chen, *ACS Nano* **2016**, *10*, 2991.
[4] a) G. Battistelli, A. Cantelli, G. Guidetti, J. Manzi, M. Montalti, *Wiley Interdiscip. Rev.: Nanomed. Nanobiotechnol.* **2016**, *8*, 139; b) J. Du, L. A. Lane, S. Nie, *J. Controlled Release* **2015**, *219*, 205.
[5] a) D. Ling, W. Park, S. J. Park, Y. Lu, K. S. Kim, M. J. Hackett, B. H. Kim, H. Yim, Y. S. Jeon, K. Na, T. Hyeon, *J. Am. Chem. Soc.* **2014**, *136*, 5647; b) P. Mi, D. Kokuryo, H. Cabral, H. Wu, Y. Terada, T. Saga, I. Aoki, N. Nishiyama, K. Kataoka, *Nat. Nanotechnol.* **2016**, *11*, 724; c) H. J. Li, J. Z. Du, X. J. Du, C. F. Xu, C. Y. Sun, H. X. Wang, Z. T. Cao, X. Z. Yang, Y. H. Zhu, S. Nie, J. Wang, *Proc. Natl. Acad. Sci. USA* **2016**, *113*, 4164.
[6] a) M. Leist, B. Single, A. F. Castoldi, S. Kuhnle, P. Nicotera, *J. Exp. Med.* **1997**, *185*, 1481; b) X. Li, X. Guo, L. Cao, Z. Xun, S. Wang, S. Li, Y. Li, G. Yang, *Angew. Chem.* **2014**, *126*, 7943; c) R. Mo, T. Jiang, R. DiSanto, W. Tai, Z. Gu, *Nat. Commun.* **2014**, *5*, 3364; d) J. Lai, B. P. Shah, Y. Zhang, L. Yang, K.-B. Lee, *ACS Nano* **2015**, *9*, 5234.
[7] Y. Zhou, F. Tozzi, J. Chen, F. Fan, L. Xia, J. Wang, G. Gao, A. Zhang, X. Xia, H. Brasher, W. Widger, L. M. Ellis, Z. Weihua, *Cancer Res.* **2012**, *72*, 304.
[8] a) Y. Wang, M. S. Shim, N. S. Levinson, H. W. Sung, Y. Xia, *Adv. Funct. Mater.* **2014**, *24*, 4206; b) X. Ai, C. J. Ho, J. Aw, A. B. Attia, J. Mu, Y. Wang, X. Wang, Y. Wang, X. Liu, H. Chen, M. Gao, X. Chen, E. K. Yeow, G. Liu, M. Olivo, B. Xing, *Nat. Commun.* **2016**, *7*, 10432.
[9] X. Ma, Y. Zhao, X. J. Liang, *Acc. Chem. Res.* **2011**, *44*, 1114.
[10] a) S. Quideau, D. Deffieux, C. Douat-Casassus, L. Pouysegu, *Angew. Chem.* **2011**, *123*, 610; b) H. Lee, S. M. Dellatore, W. M. Miller, P. B. Messersmith, *Science* **2007**, *318*, 426; c) H. Ejima, J. J. Richardson, K. Liang, J. P. Best, M. P. van Koeverden, G. K. Such, J. Cui, F. Caruso, *Science* **2013**, *341*, 154; d) Q. Ye, F. Zhou, W. Liu, *Chem. Soc. Rev.* **2011**, *40*, 4244; e) L.-S. Lin, Z.-X. Cong, J.-B. Cao, K.-M. Ke, Q.-L. Peng, J. Gao, H.-H. Yang, G. Liu, X. Chen, *ACS Nano* **2014**, *8*, 3876.
[11] a) T. S. Sileika, D. G. Barrett, R. Zhang, K. H. Lau, P. B. Messersmith, *Angew. Chem.* **2013**, *125*, 10966; b) J. Guo, Y. Ping, H. Ejima, K. Alt, M. Meissner, J. J. Richardson, Y. Yan, K. Peter, D. von Elverfeldt, C. E. Hagemeyer, F. Caruso, *Angew. Chem.* **2014**, *126*, 5652; c) J. E. Chung, S. Tan, S. J. Gao, N. Yongvongsoontorn, S. H. Kim, J. H. Lee, H. S. Choi, H. Yano, L. Zhuo, M. Kurisawa, J. Y. Ying, *Nat. Nanotechnol.* **2014**, *9*, 907.
[12] a) Z. Gao, I. Zharov, *Chem. Mater.* **2014**, *26*, 2030; b) X.-R. Song, S.-X. Yu, G.-X. Jin, X. Wang, J. Chen, J. Li, G. Liu, H.-H. Yang, *Small* **2016**, *12*, 1506.
[13] a) Y. Yuan, Z. Ding, J. Qian, J. Zhang, J. Xu, X. Dong, T. Han, S. Ge, Y. Luo, Y. Wang, K. Zhong, G. Liang, *Nano Lett.* **2016**, *16*, 2686; b) A. H. Lu, E. L. Salabas, F. Schuth, *Angew. Chem.* **2007**, *119*, 1242; c) G. Liu, J. Gao, H. Ai, X. Chen, *Small* **2012**, *9*, 1533.
[14] a) Y. W. Jun, J. W. Seo, J. Cheon, *Acc. Chem. Res.* **2008**, *41*, 179; b) R. Hao, R. Xing, Z. Xu, Y. Hou, S. Gao, S. Sun, *Adv. Mater.* **2010**, *22*, 2729; c) J. Zheng, Z. Lin, L. Zhang, H.-H. Yang, *Sci. China: Chem.* **2015**, *58*, 1056; d) J. Li, C.-Y. Hong, S.-X. Wu, H. Liang, L.-P. Wang, G. Huang, X. Chen, H.-H. Yang, D. Shangguan, W. Tan, *J. Am. Chem. Soc.* **2015**, *137*, 11210.
[15] Y. Liu, T. Chen, C. Wu, L. Qiu, R. Hu, J. Li, S. Cansiz, L. Zhang, C. Cui, G. Zhu, M. You, T. Zhang, W. Tan, *J. Am. Chem. Soc.* **2014**, *136*, 12552.
[16] a) D. G. Barrett, T. S. Sileika, P. B. Messersmith, *Chem. Commun.* **2014**, *50*, 7265; b) D. Ling, N. Lee, T. Hyeon, *Acc. Chem. Res.* **2015**, *48*, 1276.
[17] C. J. Yu, S. M. Wu, W. L. Tseng, *Anal. Chem.* **2013**, *85*, 8559.
[18] G. Wang, X. Zhang, A. Skallberg, Y. Liu, Z. Hu, X. Mei, K. Uvdal, *Nanoscale* **2014**, *6*, 2953.
[19] a) J. Gallo, N. Kamaly, I. Lavdas, E. Stevens, Q. D. Nguyen, M. Wylezinska-Arridge, E. O. Aboagye, N. J. Long, *Angew. Chem.* **2014**, *126*, 9704; b) J. M. Perez, F. J. Simeone, Y. Saeki, L. Josephson, R. Weissleder, *J. Am. Chem. Soc.* **2003**, *125*, 10192.
[20] R. Mo, T. Jiang, Z. Gu, *Angew. Chem.* **2014**, *126*, 5925.
[21] E. B. Ehlerding, F. Chen, W. Cai, *Adv. Sci.* **2016**, *3*, 1500223.
[22] a) L. Cheng, C. Wang, L. Feng, K. Yang, Z. Liu, *Chem. Rev.* **2014**, *114*, 10869; b) J. U. Menon, P. Jadeja, P. Tambe, K. Vu, B. Yuan, K. T. Nguyen, *Theranostics* **2013**, *3*, 152; c) L.-S. Lin, X. Yang, G. Niu, J. Song, H.-H. Yang, X. Chen, *Nanoscale* **2016**, *8*, 2116.

Received: November 30, 2016
Revised: February 13, 2017
Published online:

  